Monthly Notices
of the
ROYAL ASTRONOMICAL SOCIETY

MNRAS **479,** 1542–1554 (2018)
Advance Access publication 2018 May 25

doi:10.1093/mnras/sty1380

VLT/X-shooter GRBs: Individual extinction curves of star-forming regions★

T. Zafar,[1,2]† D. Watson,[3] P. Møller,[2] J. Selsing,[3] J. P. U. Fynbo,[3] P. Schady,[4] K. Wiersema,[5] A. J. Levan,[5] K. E. Heintz,[6,3] A. de Ugarte Postigo,[7,3] V. D'Elia,[8,9] P. Jakobsson,[6] J. Bolmer,[10] J. Japelj,[11] S. Covino,[12] A. Gomboc[13] and Z. Cano[6]

[1]*Australian Astronomical Observatory, PO Box 915, North Ryde, NSW 1670, Australia*
[2]*European Southern Observatory, Karl-Schwarzschild-Strasse 2, D-85748 Garching, Germany*
[3]*Dark Cosmology Centre, Niels Bohr Institute, University of Copenhagen, Juliane Maries Vej 30, DK-2100 Copenhagen, Denmark*
[4]*Max-Planck Institut für Extraterrestrische Physik, Giessenbachstrsse 1, D-85748 Garching, Germany*
[5]*Department of Physics, University of Warwick, Coventry, CV4 7AL, UK*
[6]*Centre for Astrophysics and Cosmology, Science Institute, University of Iceland, Dunhagi 5, 107 Reykjavík, Iceland*
[7]*Instituto de Astrofísica de Andalucía (IAA-CSIC), Glorieta de la Astronoma s/n, E-18008 Granada, Spain*
[8]*Space Science Data Center - Agenzia Spaziale Italiana , Via del Politecnico snc., I-00133 Roma, Italy*
[9]*Istituto Nazionale di Astrofisica – Osservatorio Astronomico di Roma, Via Frascati 33, I-00040 Monteporzio Catone, Italy*
[10]*European Southern Observatory, Alonso de Córdova 3107, Vitacura, Casilla 19001, Santiago 19, Chile*
[11]*Astronomical Institute Anton Pannekoek, University of Amsterdam, Science Park 904, NL-1098 XH Amsterdam, the Netherlands*
[12]*Osservatorio Astronomico di Brera, via Bianchi 46, I-23807 Merate (LC), Italy*
[13]*Centre for Astrophysics and Cosmology, University of Nova Gorica, Vipavska 11c, 5270 Ajdovščina, Slovenia*

Accepted 2018 May 10. Received 2018 April 5; in original form 2017 October 31

ABSTRACT

The extinction profiles in gamma-ray burst (GRB) afterglow spectral energy distributions (SEDs) are usually described by the small magellanic cloud (SMC)-type extinction curve. In different empirical extinction laws, the total-to-selective extinction, R_V, is an important quantity because of its relation to dust grain sizes and compositions. We here analyse a sample of 17 GRBs ($0.34 < z < 7.84$) where the ultraviolet to near-infrared spectroscopic observations are available through the VLT/X-shooter instrument, giving us an opportunity to fit individual extinction curves of GRBs for the first time. Our sample is compiled on the basis of the availability of multiband photometry around the X-shooter observations. The X-shooter data are combined with the *Swift* X-ray data and a single or broken power law together with a parametric extinction law is used to model the individual SEDs. We find 10 cases with significant dust, where the derived extinction, A_V, ranges from 0.1–1.0 mag. In four of those, the inferred extinction curves are consistent with the SMC curve. The GRB individual extinction curves have a flat R_V distribution with an optimal weighted combined value of $R_V = 2.61 \pm 0.08$ (for seven broad coverage cases). The 'average GRB extinction curve' is similar to, but slightly steeper than the typical SMC, and consistent with the SMC Bar extinction curve at ∼95 per cent confidence level. The resultant steeper extinction curves imply populations of small grains, where large dust grains may be destroyed due to GRB activity. Another possibility could be that young age and/or lower metallicities of GRBs environments are responsible for the steeper curves.

Key words: galaxies: high-redshift – gamma-ray burst: general – dust, extinction.

1 INTRODUCTION

'Interstellar dust' plays a crucial role in the formation of stars and the evolution and assembly of galaxies. Dust alters the light in the ultraviolet (UV) and optical wavelength ranges through scattering and absorption. Extinction provides an indirect measure of the enrichment process and conditions within an environment. Ex-

★ Based on the spectroscopic observations collected at the European Organisation for Astronomical Research in the Southern Hemisphere, 8.2 m Very Large Telescope (VLT) with the X-shooter instrument mounted at UT2 under ESO programmes 060.A-9022(C), 060.A-9427(A), 084.A-0260(B), 085.A-0009(B), 086.A-0073(B), 088.A-0051(B), 089.A-0067(B), 0.90.A-0088(B), 091.C-0934(C), and 092.A-0124(A).

† E-mail:tayyaba.zafar@aao.gov.au

tinction curve, a standard tool to study extinction as a function of wavelength, strongly depends on the dust grain size distributions and grain compositions (Weingartner & Draine 2001; Li & Draine 2001; Draine 2003).

At cosmological distances long duration gamma-ray burst (GRB) afterglows offer a unique probe to study dust in star-forming environments (e.g. Stratta et al. 2007; Li et al. 2008; Liang & Li 2009; Zafar et al. 2010; Greiner et al. 2011; Stratta, Gallerani & Maiolino 2011; Zafar et al. 2011a; Schady et al. 2012). The long duration GRBs are associated with the deaths of massive stars (e.g. Galama et al. 1998; Hjorth et al. 2003; Starling et al. 2011) and their spectral emission is synchrotron due to the interaction between the highly relativistic ejecta and surrounding interstellar medium (ISM), as explained by the fireball model (e.g. Gehrels, Ramirez-Ruiz & Fox 2009). When a GRB triggers, the *Neil Gehrels Swift Observatory* (Gehrels et al. 2004) immediately repoints its telescopes and starts observing its X-ray and UV/optical afterglow. The fast response ground-based telescopes also start obtaining photometric and spectroscopic data at multiwavelengths providing the X-ray to the near-infrared (NIR) spectral energy distributions (SEDs) for GRB afterglows. Adding X-ray data to the GRB, SED allows us to improve the constrains on the spectral slope of the afterglow emission and to model the extinction better.

A standard procedure to study dust is to fit the data with empirical extinction laws (Cardelli, Clayton & Mathis 1989; Fitzpatrick & Massa 1990; Pei 1992). The average extinction curves of the Milky Way (MW) and the large and small magellanic clouds (LMC and SMC) are different from each other due to varying strength of the rest-frame 2175 Å dust absorption feature in the former two and absence of the feature and UV-steepness in the latter case. For GRBs widely adopted extinction laws are the fixed MW, LMC, and SMC from Pei (1992) usually proving to be good for the classification of different types of extinction curves. Typically, GRB SEDs prefer fixed SMC featureless extinction law (e.g. Zafar et al. 2011a) from Pei (1992) with $R_V = 2.93$ (total-to-selective extinction). However, in some cases adjustable parametric laws (Fitzpatrick & Massa 1990) are proven to best match the data (Elíasdóttir et al. 2009; Perley et al. 2011; Schady et al. 2012; Zafar et al. 2012). In the parametric extinction laws, the R_V parameter is of particular interest as its small value defines a steep extinction curve and vice versa. The steepness and flatness of the extinction curve are related to the dust grain size distribution and composition (Weingartner & Draine 2001) making this quantity pivotal to understand the dust properties.

With the advancements of various instruments such as the VLT/X-shooter (Vernet et al. 2011), the spectra of GRB afterglows are now available at multiwavelengths. X-shooter spectrograph has simultaneous coverage from the UV to the NIR through three spectroscopic arms: UVB (300–550 nm), VIS (550–1000 nm), and NIR (1000–2500 nm). This broader coverage and the availability of the X-ray data provide us with an opportunity to fit the individual extinction curves of GRB afterglows rather than using fixed laws to understand dust properties at higher redshifts.

In Section 2 we present our sample selection criteria and provide details about the multiwavelength data. In Section 3 we describe our parametric dust law and SED analysis. Our results are presented in Section 4, and a discussion and conclusions are provided in Sections 5 and 6. Throughout the paper, errors donate 1σ uncertainties unless stated otherwise.

2 DATA SAMPLE

2.1 Sample selection

Under the X-shooter GRB target of opportunity (ToO) programs, spectra for a large sample of GRB afterglows have been acquired from 2009 March to 2014 March. The spectra are reduced and flux calibrated using the standard X-shooter pipeline (version 2.0, Modigliani et al. 2010). The X-shooter GRB afterglow spectra are taken usually with slit widths of 1.0, 0.9, and 0.9 arcsec for UVB, VIS, and NIR spectra, respectively. A detailed description on the reduction and flux calibration of the spectra will be presented in Selsing et al. (2018) describing the data reduction including background subtraction, extraction, and flux calibration. Our parametric dust extinction analysis is, in particular, sensitive to flux calibration. For the GRB afterglow data, two factors could lead to sub-optimal flux calibration, i.e.: *(i)* The flux standard star observations for X-shooter are taken with a broader 5.0 arcsec wide slit and hence has different slit loss than the science spectra, and *(ii)* Atmospheric dispersion correctors (ADC) for the UVB and VIS arms were disabled from 2012 August and until recently – after our latest spectra were secured. Therefore, we cannot solely rely on the instrument's response function and we hence require photometric data around each X-shooter observations. We looked into the literature for multiband photometric data available around each X-shooter observation. We further selected the cases where data is either not affected or corrected for the contamination by the supernova or GRB host galaxy emission. This criterion leaves us with a sample of 17 long duration GRB afterglows with redshifts ranging from $0.34 < z < 7.84$ to conduct the NIR to X-ray SED analysis and derive extinction curves from the star-forming regions.

Previously, Japelj et al. (2015) fitted the X-ray to the X-shooter SEDs of nine GRB afterglows using fixed Local Group Pei (1992) extinction laws and binned X-shooter data. Eight members of our sample overlap with their sample (except short GRB 130603B), however, we here attempt to fit a free parametric dust model to derive individual extinction curves for the *unbinned* X-shooter data for the first time. Our method keeps the original spectral binning of X-shooter and no additional binning during the SED construction process is applied. The overlapping cases are discussed individually in Section 4.

2.2 X-shooter data

The X-shooter spectra together with photometric data were corrected for the foreground Galactic extinction (see Table 1) using the Galactic maps of Schlafly & Finkbeiner (2011). The Galactic extinction is usually small with $E(B-V) \lesssim 0.15$ therefore the uncertainty on this value should have a negligible effect on our final results. The X-shooter spectra were then normalized to the level of the photometric observations to generate SEDs at the photometry mid-time, Δt. The UVB and VIS arm data are comparable with the photometry within ∼10 per cent and the NIR data usually differ by 15–20 per cent from the photometry. The HEASOFT software (version 6.19) tool `flx2xsp` was used to generate XSPEC (version12.9; Arnaud 1996) readable spectral (PHA) and response matrices (RSP) files for the X-shooter data. A background file was then created to mask out non-required data channels. In detail: (i) to prevent contamination caused by the damped Lyα absorber and Lyα forest, entire blueward and some redward data (to avoid H I damping wing) around $\lambda_{\rm rest} < 1216$ Å is excluded , (ii) regions of emission and absorption lines arising from different metal species and atmospheric

Table 1. The X-shooter GRB afterglow sample. The columns indicate: *(i)* GRB name, *(ii)* redshift, *(iii)* Galactic extinction, *(iv)* total Galactic equivalent neutral hydrogen column density, and *(v)* midtime of the SED.

GRB	z	$E(B-V)_{\rm Gal}$ mag	$N_{\rm H,Gal}$ 10^{20} cm^{-2}	Δt days
090 313	3.372	0.03	2.10	1.74
090926A	2.106	0.02	2.97	0.89
100219A	4.667	0.07	6.50	0.55
100316B	1.180	0.12	9.92	0.05
100418A	0.624	0.06	6.08	1.47
100814A	1.440	0.02	1.85	4.10
100901A	1.408	0.09	9.49	2.76
101219B	0.552	0.02	3.32	0.48
111008A	4.991	0.01	0.99	0.41
111209A	0.677	0.02	1.54	0.90
120119A	1.728	0.10	11.3	0.07
120815A	2.358	0.10	11.9	0.08
120923A	7.840	0.13	15.1	0.78
121024A	2.298	0.09	7.87	0.13
130427A	0.339	0.02	1.91	0.65
130606A	5.913	0.02	2.14	0.33
131117A	4.042	0.02	1.50	0.02

telluric lines are removed, and (iii) bad spikes originating from the sky subtraction residuals (usually in the NIR arm) are masked out to obtain clean continuum data. The PHA, RSP, and background files were then grouped using the `grppha` tool without any binning applied to individual data channels.

2.3 X-ray data

The *Swift* X-ray Telescope (XRT, Burrows et al. 2005) obtained observations of each GRB afterglow. The X-ray light curves were obtained from the *Swift* online repository (Evans et al. 2009) and a decay model (Beuermann et al. 1999) is fitted. The X-ray spectrum in the 0.3–10.0 keV energy range for each GRB afterglow around the X-shooter spectra mid-time Δt was reduced using the HEASOFT software. We verified that the X-ray data show no evidence of spectral evolution so that the light curve hardness ratio around Δt is not deviating from the mean. We used photon counting (PC) mode data and extracted spectral files using the XSELECT (version 2.4) tool. Response matrices were used from the *Swift* XRT calibration files. The X-ray spectral files were grouped to 20 counts per energy channel using the `grppha` tool. Using the X-ray light curves, the flux of the X-ray data were normalized to the SED mid-time, Δt, by taking the ratio of the flux level at the SED time and the photon weighted mean time of the X-ray spectrum. For this purpose the `fparkey` command keyword EXPOSURE is used to correct the 0.3–10.0 keV flux level.

3 SED ANALYSIS

The rest-frame X-ray through *unbinned* optical/NIR instantaneous SEDs of the GRB afterglows were fitted within the spectral fitting package XSPEC using a single or broken power law together with a parametric extinction law to model for dust.

The continuum emission from the GRB afterglow is dominated by synchrotron radiation and a single power-law case described as $F_\nu = F_0 \nu^{-\beta_1}$. Here F_0 is the normalization flux, ν is the frequency, and β_1 is the intrinsic spectral slope. In case of a broken power-law model a cooling break, $\nu_{\rm break}$, is introduced and the law is described by two slopes, β_1 (optical slope) and β_2 (X-ray slope), as

$$F_\nu = \begin{cases} F_0 \nu^{-\beta_1} & \nu \leq \nu_{\rm break} \\ F_0 \nu_{\rm break}^{\beta_2-\beta_1} \nu^{-\beta_2} & \nu \geq \nu_{\rm break} \end{cases} \quad (1)$$

In the latter case, the cooling break was modelled such that the change in slope, $\Delta\beta$, was fixed at 0.5 (Sari, Piran & Narayan 1998). Such a change in the spectral indices is supported by the analysis of Zafar et al. (2011a) for a spectroscopic sample of GRBs (see also Greiner et al. 2011, for a photometric sample analysis).

The XSPEC models *phabs* and *zphabs* were used to correct the foreground Galactic and host galaxy photoelectric absorptions in the X-ray data. The total Galactic equivalent neutral hydrogen column density, $N_{\rm H,Gal}$, was fixed to the values calculated from Willingale et al. (2013). Willingale et al. (2013) investigated the biases and completeness of the atomic hydrogen column density reported by Kalberla et al. (2005), and included the contribution from molecular hydrogen (Wilms, Allen & McCray 2000) and Galactic dust (Schlegel, Finkbeiner & Davis 1998) to that. This results in higher $N_{\rm H,Gal}$ values and carry no systematic errors to our final results. Another prescription to estimate the total Galactic column density based on dust maps was proposed by Watson (2011). We use the Willingale et al. (2013) values because they provide higher Galactic columns. The host galaxy equivalent neutral hydrogen column density from the soft X-ray absorption, $N_{\rm H,X}$, is left as a free parameter. The XSPEC default solar abundances of Anders & Grevesse (1989) are used following the discussions of Watson (2011) and Watson et al. (2013).

3.1 Dust model

The optical afterglow is extinguished due to dust absorption and scattering along the line of sight and observed spectra are changed to: $F_\nu^{\rm obs} = F_\nu 10^{-0.4A_\lambda}$, where A_λ is the wavelength dependent extinction curve. We use the Fitzpatrick & Massa (1990) law providing freedom to generate extinction curves with eight free parameters. It contains the galaxy dust extinction, A_V, the total-to-selective dust extinction, R_V , and six coefficients defining: (i) the UV linear component specified by c_1 (intercept) and c_2 (slope), (ii) the height (c_3), width (γ), and central wavelength (x_0) of the 2175 Å bump, which is modelled with a Lorentzian-like Drude component (Bohren & Huffman 1983), (iii) and the far-UV curvature term defined by $F(\lambda^{-1})$ and far-UV parameter c_4. The extinction properties in the IR and optical ranges are determined using spline interpolation points. The wavelength-dependent extinction is then given as

$$A_\lambda = \frac{A_V}{R_V} \times \left[c_1 + c_2\lambda^{-1} + c_3 D(x, x_0, \gamma) + c_4 F(\lambda^{-1}) + 1\right], \quad (2)$$

where $F(\lambda^{-1}) = 0$ for $\lambda^{-1} < 5.9\,\mu{\rm m}^{-1}$ and $F(\lambda^{-1}) = 0.5392\,(\lambda^{-1} - 5.9)^2 + 0.05644\,(\lambda^{-1} - 5.9)^3$ for $\lambda^{-1} \geqslant 5.9\,\mu{\rm m}^{-1}$. Hereafter, we will refer to this extinction model as FM. We first fit the data with all parameters (including Drude component), but find that not in a single case the c_3 parameter is significantly different from zero. This suggests that the 2175 Å extinction bump is not present for our GRB afterglow sample. We therefore fix the bump parameters c_3, γ, and x_0 to 0, 1.0, and 4.6 $\mu{\rm m}^{-1}$, respectively. This is done to avoid degeneracies of bump parameters (c_3, γ, and x_0) when significant bump is not present following the discussions of Zafar et al. (2015). Zafar et al. (2015) tested the SMC-Bar value of $c_3 = 0.389$ from Gordon et al. (2003) and $c_3 = 0$, finding a decrease in χ^2 values with $c_3 = 0$.

In simultaneous SED analysis within XSPEC, c_1, c_2, c_4, A_V, R_V, host metal absorption ($N_{\rm H,X}$), and spectral indices of the continuum

(β_1 and β_2), were fitted as free parameters for each GRB afterglow. The best-fitting results for each GRB and the resulting χ^2 are provided in the Table 2. We considered a broken power-law model to provide a better fit to the afterglow SED when the F-test probability is smaller than 5 per cent . This slightly higher F-test probability threshold is chosen due to relatively higher uncertainties on the X-shooter spectra to avoid the wrong classification of an SED having a single power law. An incorrect classification could affect the best-fitting A_V and hence R_V values. However, for broken power law cases we always find probability smaller than 1 per cent .

4 RESULTS

We used the X-shooter GRB SEDs to generate individual extinction curves. Note that the photometric data are only used to normalize the X-shooter data to avoid flux calibration discrepancies. The SED fits are only performed on the *unbinned* X-shooter and binned XRT data. The best-fitting SEDs of GRB afterglows in our sample and extinction curves with their 1σ uncertainties for dusty cases (in insets) are shown in Fig. 1. As a comparison, we plot the canonical Pei (1992) SMC extinction curve in the insets. Spectroscopic and photometric data collection, SED generation, and comparison with previous studies are outlined in this section on a case by case basis.

4.1 GRB 090313

The X-shooter spectra of GRB 090313 ($z = 3.372$) were taken at 1.88 d after the burst trigger during the instrument commissioning. The photometric data at 1.74 d after the burst in the $r'I$ and J bands are taken from the light curves provided by Melandri et al. (2010). The X-shooter spectra were normalized to the optical/NIR photometric data at 1.74 d. The SED fits well with a single power law and a featureless extinction curve ($R_V = 2.67^{+0.13}_{-0.17}$) with $A_V = 0.3 \pm 0.06$. Previously, Kann et al. (2010) fitted the optical/NIR SED suggesting an SMC-type curve with $A_V = 0.34 \pm 0.15$, consistent to our extinction value.

4.2 GRB 090926A

The X-shooter spectra of the GRB 090926A ($z = 2.016$) afterglow were taken at 0.917 d after the burst trigger. The Gamma-Ray Burst Optical and Near-Infrared Detector (GROND) photometry in the $g'r'i'$ and z' bands are available from Rau et al. (2010) at 0.891 days after the burst. Due to technical issues, GROND *JH*-and *K*-band photometry are not available near the epoch of the X-shooter observations. We scaled the X-shooter spectra to the optical photometric data at 0.891 d. The X-shooter to X-ray SED prefers a single power law and no dust extinction with $A_V < 0.04$. Previously Rau et al. (2010) and D'Elia et al. (2010) also reported no dust extinction for this burst with $A_V < 0.1$ and $A_V < 0.03$, respectively.

4.3 GRB 100219A

The X-shooter UVB to NIR spectra of GRB 100219A ($z = 4.667$) were obtained at 0.55 d after the burst trigger. Photometric data for SED normalization are obtained from Thöne et al. (2013) in the $i'z'JH$- and *K*-bands from GROND. The SED fits well with a single power law and featureless extinction curve ($R_V = 2.65 \pm 0.09$) with $A_V = 0.14 \pm 0.03$. Previously Thöne et al. (2013) found best-fitting with an SMC-type extinction curve and $A_V = 0.13 \pm 0.05$ using the X-shooter spectrum at similar epoch, suggesting consistent results. In contrast, Japelj et al. (2015) claimed the X-shooter to X-ray SED fits well with an LMC extinction curve with $A_V = 0.23 \pm 0.02$. We do not find any evidence of 2175 Å the bump (with $c_3 < 0.26$) in the spectrum and a slightly higher extinction. Recently, Bolmer et al. (2018) found an SMC-type curve with $A_V = 0.15^{+0.04}_{-0.05}$ could explain the GROND-XRT SED, consistent with our results.

4.4 GRB 100316B

At ∼0.045 d after the burst, the X-shooter spectra of the GRB 100316B ($z = 1.180$) afterglow were taken. The photometric data for this afterglow are taken from Haislip et al. (2010) with the Panchromatic Robotic Optical Monitoring and Polarimetry Telescopes (PROMPT) at Cerro Tololo Inter-American Observatory (CTIO) in the *BVR*, and *I* bands. The X-shooter data were scaled to the photometry at ∼0.05 d after the burst. The X-shooter to X-ray SED fits well with a broken power law (with the break significance is <99 per cent) and no dust extinction with $A_V < 0.09$. Previously Greiner et al. (2011) found that a broken power law with $A_V < 0.15$ provides the best solution to the GROND-XRT SED.

4.5 GRB 100418A

The X-shooter observations of GRB 100418A ($z = 0.624$) were carried out at 0.4, ∼1.5, and 2.4 d after the burst. The first two epochs have good flux calibration and the third epoch spectra have contamination from the GRB host galaxy and supernova emission. The NIR data of the first epoch has low S/N in the *K*-band. We therefore used the second epoch observations for our SED analysis due to having better NIR data. Photometric data for the SED normalization were obtained with GROND in all seven bands from de Ugarte Postigo et al. (2018). We find that SED fits well with a single power law and $A_V = 0.12 \pm 0.03$ with a featureless extinction curve with $R_V = 2.42^{+0.08}_{-0.10}$. Note that even with lesser NIR data, the dust content at the first two epochs remains $A_V \sim 0.12$. de Ugarte Postigo et al. (2011) derived intrinsic extinction of $A_V = 0.09 \pm 0.04$ with an SMC law using the X-shooter spectra. Japelj et al. (2015) found the best-fitting with a broken power law and $A_V = 0.20^{+0.03}_{-0.02}$ with an SMC extinction curve for the X-shooter-XRT SED at a similar epoch as ours. Japelj et al. (2015) reported a break in the optical data. However, Marshall et al. (2011) find no evidence of a spectral break in the NIR-to-X-ray light curves after rebrightening at ∼0.6 d, consistent with our findings.

4.6 GRB 100814A

The X-shooter spectra of GRB 100814A ($z = 1.440$) were obtained at ∼0.04, ∼0.09, and 4.1 d after the burst trigger. Due to flux calibration discrepancy at earlier two epochs, the data at 4.1 d after the burst are analysed here. Photometric data from Nardini et al. (2014) taken with GROND in all seven bands are used for the SED normalization. The X-ray to the NIR SED fits well with a single power law and no dust extinction with $A_V < 0.07$. Nardini et al. (2014) fitted the GROND-XRT SEDs at four epochs simultaneously with a constant value of extinction and obtained $A_V < 0.04$ with an SMC curve, consistent with our results. Japelj et al. (2015) fitted the X-shooter-XRT SED and found the best-fitting with a broken power law and an SMC extinction curve with $A_V = 0.20 \pm 0.03$. The spectral break was found within the optical data. Nardini et al. (2014) found a spectral break evolution by fitting SEDs at four different epochs where the latter case at ∼5 d is consistent with single power law. This is consistent with our results suggesting no spectral break in the optical data.

Table 2. Results of the FM best-fitting parameters for the GRB afterglow X-ray to X-shooter SEDs. The columns give the burst name, the equivalent neutral hydrogen column density $N_{\rm H,X}$, optical slope β_1, X-ray slope β_2, break frequency $\nu_{\rm break}$, UV linear component intercept c_1, UV linear component slope c_2, far-UV curvature c_4, total-to-selective extinction R_V, dust content A_V, reduced χ^2 together with number of degrees of freedom (dof) and the null hypothesis probability (NHP) for the best-fitting model, and F-test probability to compare single and broken power-law models. The second-last row provides the weighted mean values and 1σ errors of all extinction curves parameters. The standard deviations around the weighted mean values are provided in the last row.

GRB	$N_{\rm H,\,X}$ 10^{22} cm^{-2}	β_1	β_2	log $\nu_{\rm break}$ Hz	c_1 μm	c_2 μm^2	c_4	R_V	A_V mag	χ^2_ν/dof (NHP per cent)	F-test prob.
090 313	$4.23^{+1.61}_{-2.10}$	$1.18^{+0.12}_{-0.16}$			-4.92 ± 0.09	2.10 ± 0.10	0.49 ± 0.07	$2.67^{+0.13}_{-0.17}$	0.30 ± 0.06	0.92/21759(100)	0.96
090926A	$0.55^{+0.31}_{-0.18}$	$0.82^{+0.09}_{-0.11}$							<0.04	0.97/28733(100)	1.00
100219A	<6.67	$0.55^{+0.06}_{-0.07}$			-5.16 ± 0.03	2.37 ± 0.05	1.48 ± 0.08	$2.65^{+0.09}_{-0.09}$	0.14 ± 0.03	1.02/17021(2.85)	1.00
100316B	<0.43	$0.58^{+0.08}_{-0.09}$	$1.08^{+0.05}_{-0.04}$	16.67 ± 0.06					<0.09	1.03/36438(0.04)	0.01
100418A	$0.28^{+0.19}_{-0.12}$	$1.01^{+0.12}_{-0.10}$			-5.37 ± 0.07	2.30 ± 0.06	0.68 ± 0.09	$2.42^{+0.08}_{-0.10}$	0.12 ± 0.03	0.86/34588(100)	0.84
100814A	$0.21^{+0.10}_{-0.08}$	$0.92^{+0.12}_{-0.08}$							<0.07	0.98/33495(99.7)	1.00
100901A	$0.22^{+0.12}_{-0.10}$	$0.70^{+0.13}_{-0.16}$	$1.20^{+0.11}_{-0.08}$	15.73 ± 0.07	-3.57 ± 0.07	2.04 ± 0.05	0.04 ± 0.08	$3.01^{+0.11}_{-0.11}$	0.25 ± 0.08	1.03/31421(0.05)	<0.01
101219B	$0.08^{+0.05}_{-0.03}$	$0.93^{+0.14}_{-0.10}$							<0.11	0.96/41338(100)	1.00
111008A	$2.14^{+1.18}_{-1.03}$	$0.47^{+0.06}_{-0.06}$	$0.97^{+0.05}_{-0.07}$	16.25 ± 0.08	-4.84 ± 0.07	2.36 ± 0.05	0.44 ± 0.06	$2.47^{+0.07}_{-0.09}$	0.12 ± 0.04	0.92/22541(100)	0.01
111209A	$0.16^{+0.06}_{-0.05}$	$0.68^{+0.12}_{-0.09}$	$1.18^{+0.08}_{-0.09}$	16.12 ± 0.11	-5.12 ± 0.11	2.28 ± 0.08	0.72 ± 0.06	$2.53^{+0.13}_{-0.15}$	0.18 ± 0.08	1.01/38817(16.9)	<0.01
120119A	$0.94^{+0.66}_{-0.42}$	$0.84^{+0.10}_{-0.09}$			-4.13 ± 0.08	2.09 ± 0.07	0.22 ± 0.10	$2.99^{+0.24}_{-0.18}$	1.02 ± 0.11	0.91/36437(100)	0.84
120815A	<0.97	$0.92^{+0.10}_{-0.10}$			-4.77 ± 0.08	2.14 ± 0.07	0.82 ± 0.08	$2.38^{+0.09}_{-0.09}$	0.19 ± 0.04	1.02/31427(0.60)	1.00
120923A	<26.1	$0.91^{+0.10}_{-0.21}$							<0.16	0.93/5302(100)	0.59
121024A	<1.47	$0.85^{+0.09}_{-0.13}$			-4.23 ± 0.06	2.20 ± 0.08	0.57 ± 0.05	$2.81^{+0.20}_{-0.16}$	0.26 ± 0.07	1.02/29533(0.44)	0.98
130427A	$0.08^{+0.02}_{-0.02}$	$0.74^{+0.04}_{-0.04}$			-5.06 ± 0.10	2.24 ± 0.09	0.42 ± 0.07	$2.92^{+0.19}_{-0.14}$	0.11 ± 0.04	0.94/30432(100)	1.0
130606A	<4.10	$0.96^{+0.05}_{-0.12}$							<0.07	0.98/26351(99.6)	1.0
131117A	<1.78	$0.42^{+0.11}_{-0.09}$	$0.92^{+0.06}_{-0.08}$	15.95 ± 0.13					<0.11	0.95/30278(100)	<0.01
WM					-4.83 ± 0.08	2.23 ± 0.05	0.59 ± 0.02	2.59 ± 0.07			
Stddev					0.22	0.15	0.06	0.21			

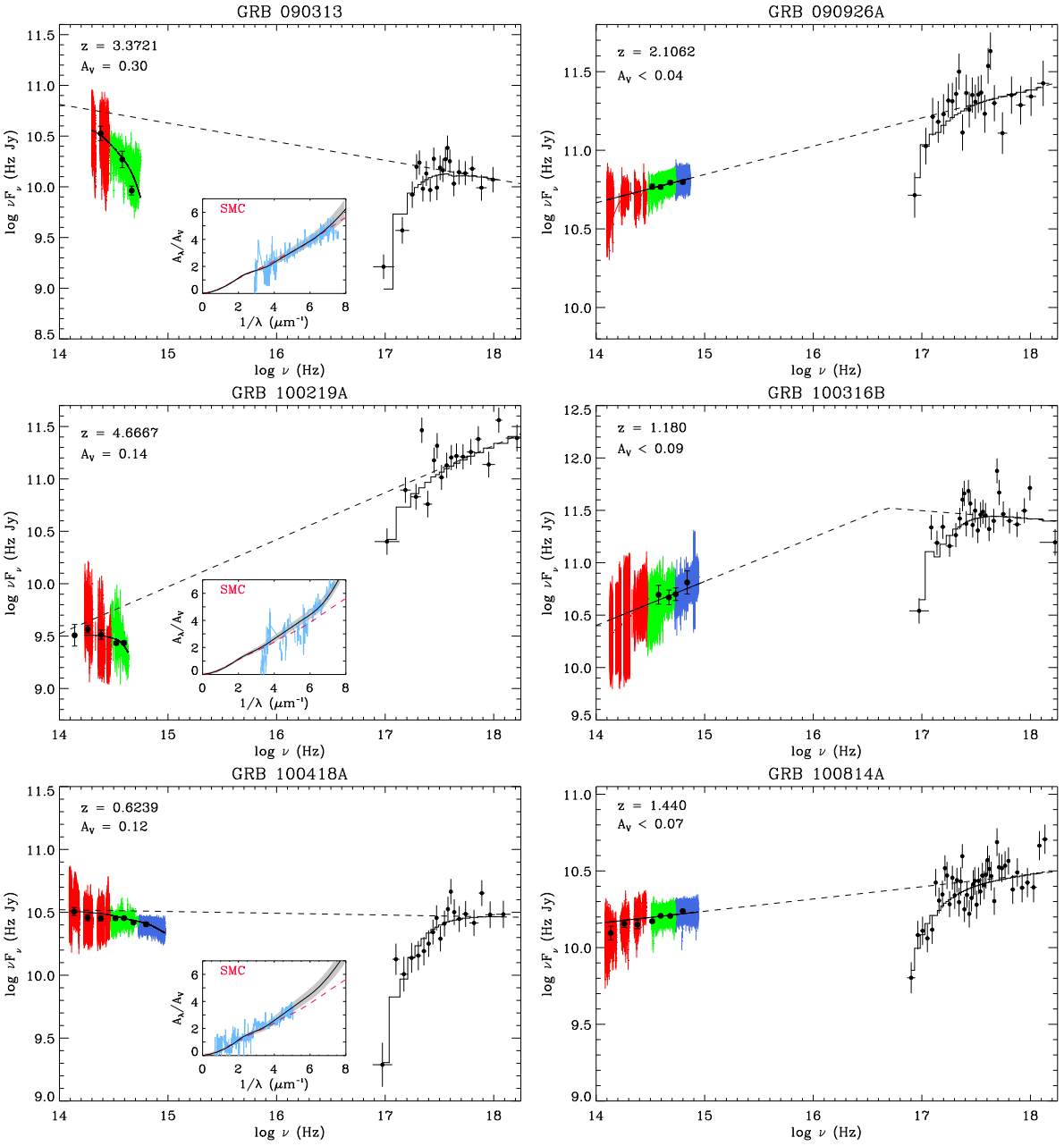

Figure 1. The observed-frame VLT/X-shooter GRB afterglow SEDs and their best-fitting models. In each panel, the *Swift* X-ray data on the right side is indicated by black points. The blue, green, and red colours correspond to the UVB, VIS, and NIR spectra from the VLT/X-shooter, respectively. Black overlaid points on the X-shooter spectra are the photometric data from different sources (see Section 4). The errors on the spectroscopic and photometric data are also plotted. The X-shooter spectra are binned for visual purposes. The best-fitting extinguished (solid lines) and extinction corrected spectral models (dashed lines) are shown in black. *Inset:* For extinguished cases, the best-fitting absolute extinction curves of the GRBs are shown with black lines together with their 1σ uncertainty with grey shaded area. The cyan curves represent the X-shooter spectra. The red dashed line corresponds to the canonical SMC extinction curve from Pei (1992).

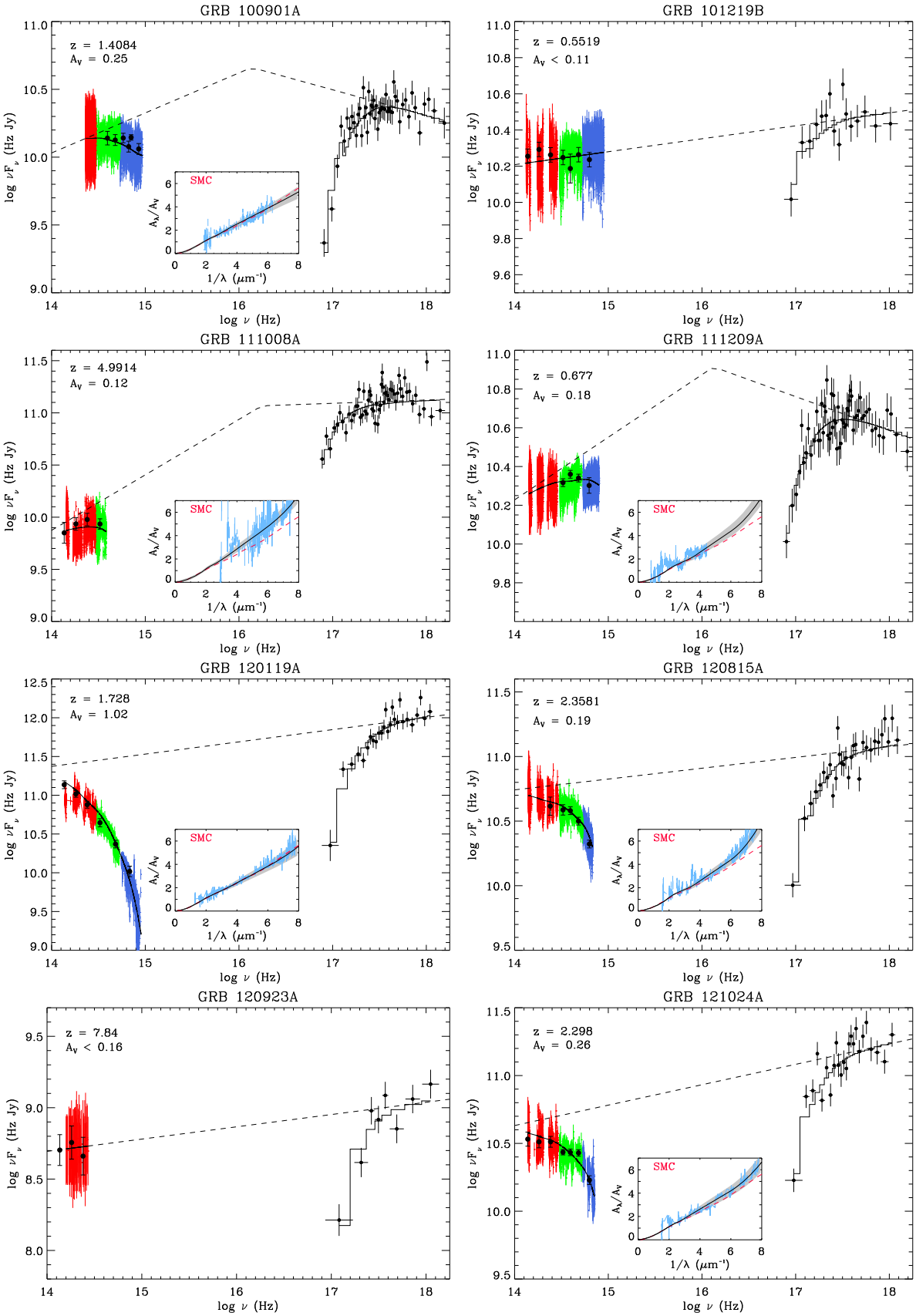

Figure 1. *– continued.*

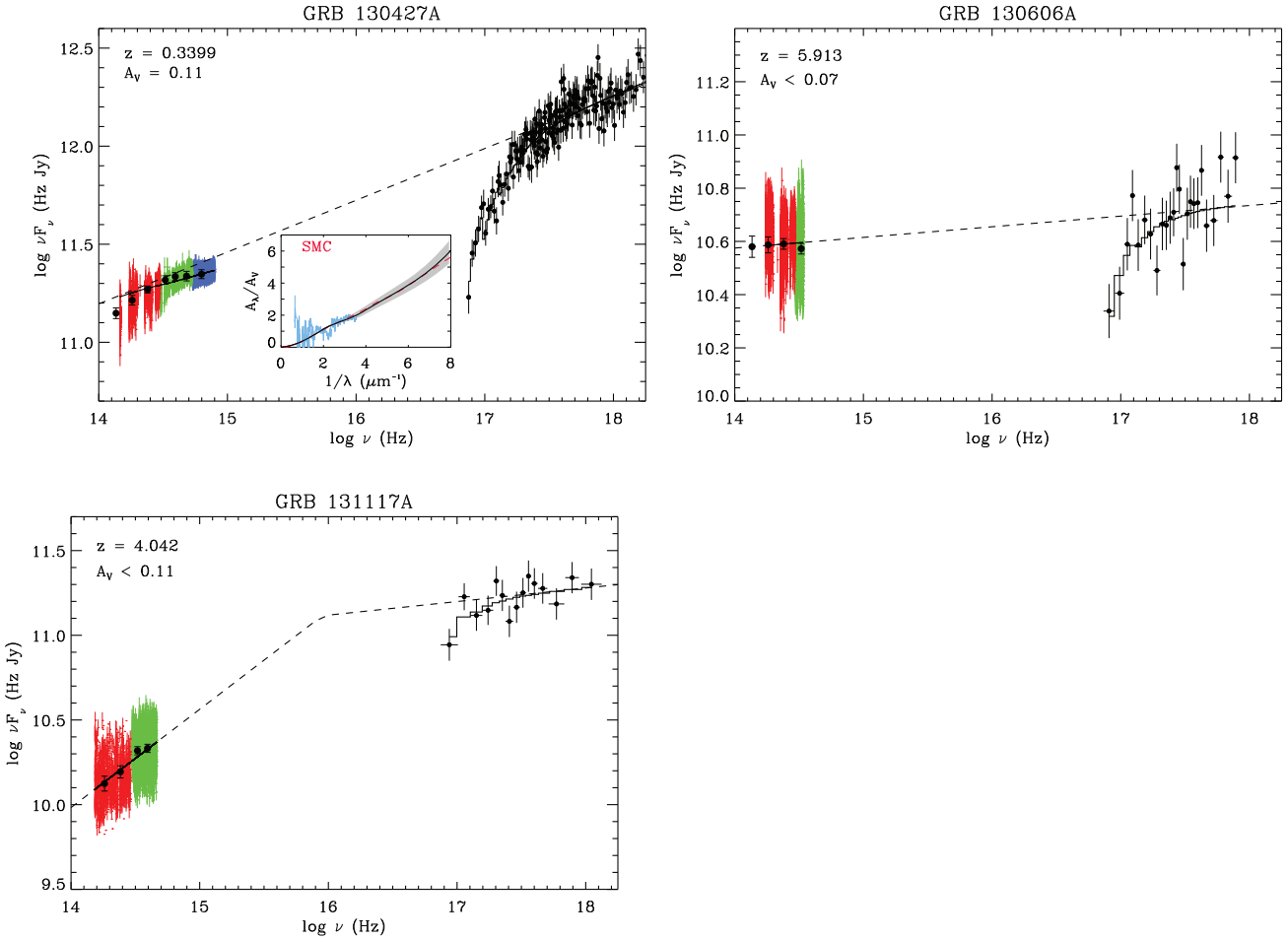

Figure 1. – *continued.*

4.7 GRB 100901A

The X-shooter spectra of GRB 100901A ($z = 1.408$) were acquired at 2.758 d after the burst trigger. For SED normalization, photometric data are taken from Gomboc et al. (in preparation). The NIR to X-ray SED fits well with a broken power law and $A_V = 0.25 \pm 0.08$ and prefers a flatter extinction curve with $R_V = 3.01 \pm 0.11$. Previously, Hartoog et al. (2013), using the photometric SED from Gomboc et al. (in preparation), derived $A_V = 0.21$. Japelj et al. (2015) reported a broken power law with an SMC extinction curve provides the best-fitting to these data with $A_V = 0.29 \pm 0.03$, consistent with our values.

4.8 GRB 101219B

The X-shooter spectra of the afterglow of GRB 101219BA ($z = 0.552$) were taken at three epochs at 0.483, 16.4, and 39.6 d after the burst. We used the first epoch at 0.483 d after the burst for the SED analysis as the other two epoch spectra have SN contamination (Sparre et al. 2011). Photometric data from GROND in all seven bands are available at the first epoch (Sparre et al. 2011) and used for the spectra normalization. The SED provides a good fit with a single power law and no dust extinction with $A_V < 0.11$. Sparre et al. (2011) also found no dust extinction for the similar data with $A_V < 0.1$.

4.9 GRB 111008A

The X-shooter spectra of GRB 111008A ($z = 4.991$) were taken at ∼0.355 d after the burst trigger. GROND photometry in the $z'JH$- and K-bands are available at 0.41 d after the burst from Sparre et al. (2014). We normalized the X-shooter spectra to the level of the GROND photometry to fit for intrinsic extinction curve. The SED prefers a broken power law and a featureless steep extinction curve ($R_V = 2.47^{+0.07}_{-0.08}$) with $A_V = 0.12 \pm 0.04$. Sparre et al. (2014) found that the GROND-XRT data fitted well with a broken power law and an SMC extinction curve with $A_V = 0.11 \pm 0.04$. Recently, Bolmer et al. (2018) suggested that the GRB photometric SED can be explained by an SMC-type curve with $A_V = 0.13^{+0.03}_{-0.07}$, both findings consistent with our extinction values.

4.10 GRB 111209A

The X-shooter spectra of GRB 111209A ($z = 0.677$) afterglow were taken at 0.74 and 19.82 d after the burst. We used the first epoch

spectra for the SED analysis where the Gemini-North photometric observations in the *gri* and *z* bands are available at 0.90 d after the burst from Levan et al. (2014). After the normalization, the SED at 0.90 d fits well with a broken power law and a featureless extinction curve ($R_V = 2.53^{+0.13}_{-0.15}$) with a visual extinction of $A_V = 0.18 \pm 0.08$. Previously, Stratta et al. (2013) performed multi-epoch SED analysis and reported that the GRB afterglow can be explained with dust extinction of $A_V = 0.3$–1.5, that may undergo dust destruction at late times.

4.11 GRB 120119A

The X-shooter spectra of GRB 120119A ($z = 1.728$) were obtained at ∼0.074 and 0.2 days after the burst trigger. We here use the X-shooter observations taken at 0.074 d after the burst due to better signal-to-noise. Photometric data for SED normalization are obtained from Morgan et al. (2014) in the *B-*, *R-*, *I-*, *J-*, *H-* and *K*-bands. The SED fits well with a single power law and featureless SMC-like extinction curve ($R_V = 2.97^{+0.19}_{-0.22}$) with $A_V = 1.02 \pm 0.11$. This burst has the highest amount of extinction in our sample. For such a high extinction usually 2175 Å bumps are seen (Zafar et al. 2011a; Schady et al. 2012). Due to the redshift of the burst the location of a 2175 Å bump would be between the UVB and VIS arm data. The reduction is poor in those regions due to instrumental effect and excluding those regions, the SED fit provides a bump strength of $c_3 < 0.43$. Previously Morgan et al. (2014) found the best-fitting with an SMC-type extinction curve and $A_V = 0.88 \pm 0.01$ for this burst at ∼39 min after the burst. Later, using the X-shooter spectrum Japelj et al. (2015) found that none of the standard extinction curves can fit the data well and extinction for this burst is $A_V = 1.07 \pm 0.03$.

4.12 GRB 120815A

The X-shooter spectra of GRB 120815A ($z = 2.358$) afterglow were taken at 0.086 d after the burst trigger. The GROND afterglow photometry is available at 0.084 d after the burst in the $g'r'i'z'$ and *J-*, where g'-band data is affected by the Lyα absorption (Krühler et al. 2013). We normalized our spectra to the available photometry. Our SED fits well with a single power law and the steepest extinction curve of our sample $R_V = 2.38 \pm 0.09$ and $A_V = 0.19 \pm 0.04$. Krühler et al. (2013) found that the GROND-X-ray SED fit prefers an SMC extinction law with $A_V = 0.15 \pm 0.02$, consistent with our results. However, with the X-shooter spectra, Japelj et al. (2015) found that an SMC law with $A_V = 0.32 \pm 0.02$ provides the best solution to these data. Such higher extinction value could be a result of using fixed law and finding a break in the optical data. In contrast, Krühler et al. (2013) reported an absence of spectral break from the NIR-to-X-ray light-curves analysis.

4.13 GRB 120923A

The spectrum of the highest redshift burst (GRB 120923A: $z = 7.840$) of our sample was taken with the X-shooter at 0.82 d after the burst trigger. The X-shooter spectrum shows GRB trace redward of 1200 nm therefore only NIR arm observations are used for the SED analysis. At 0.789 d after the burst, photometric data in the *J-*, *H-*, and K_s-band were taken with the VLT Infrared Spectrometer And Array Camera (ISAAC) reported by Tanvir et al. (2017). We normalized the X-shooter-XRT observations to the photometric data. The SED at 0.789 days after the burst fits well with a single power-law and no extinction with $A_V < 0.16$. Tanvir et al. (2017) reported marginal to no dust extinction with $A_V < 0.2$ from a separate photometric and spectroscopic analysis, consistent with our findings.

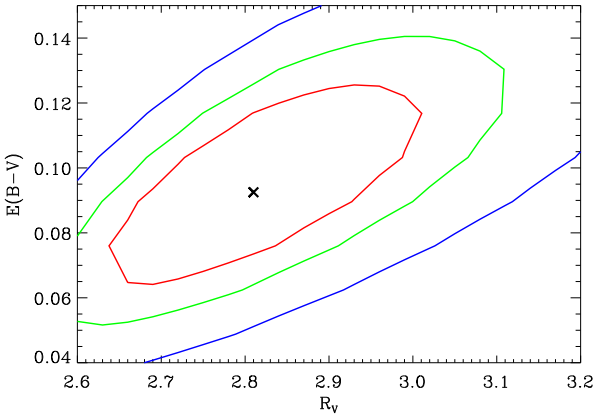

Figure 2. 1σ (red), 2σ (green), and 3σ (blue) contours for the dust extinction, $E(B-V)$, and total-to-selective extinction, R_V, are shown for the case of GRB 121024A.

4.14 GRB 121024A

The X-shooter spectra of GRB 121024A ($z = 2.298$) were acquired at ∼0.075 d after the burst. Photometric data for the SED normalization were obtained with GROND in all seven bands (Wiersema et al. 2014; Varela et al. 2016). The SED is generated at 0.128 d after the burst. The SED fits well with a single power law and featureless extinction curve ($R_V = 2.81^{+0.20}_{-0.16}$) with $A_V = 0.26 \pm 0.07$ (see Fig. 2 as an example of the quality of the fit). Previously, Wiersema et al. (2014) and Varela et al. (2016) found the best-fitting value of $A_V = 0.22 \pm 0.02$ and $A_V = 0.18 \pm 0.04$, respectively with an SMC-type extinction curve. Using the dust-to-metals correction, Friis et al. (2015) expected an extinction of $A_V = 0.9 \pm 0.3$ requiring $R_V > 15$. However, their GROND-XRT data fits well with an SMC extinction model with $A_V = 0.09 \pm 0.02$.

4.15 GRB 130427A

The X-shooter spectra of GRB 130427A ($z = 0.339$) were taken at 0.52 d after the burst (Xu et al. 2013). The photometric data in the $g'r'i'z'JH$ and *K* bands at ∼0.65 d after the burst are taken from the light curves provided by Perley et al. (2014). The SED is scaled to the photometry level at 0.65 d. The SED provides a good fit with a single power law and a featureless extinction curve ($R_V = 2.92^{+0.19}_{-0.14}$) with a small amount of extinction $A_V = 0.11 \pm 0.04$. Perley et al. (2014) performed radio to the 100 GeV *Fermi* Large Area Telescope (LAT) SED fits at different epochs and reported that the optical/NIR data prefers an SMC extinction curve with $A_V = 0.13 \pm 0.06$, consistent with our results. However, Japelj et al. (2015) suggested an SMC curve with $A_V = 0.16 \pm 0.02$ and a broken power law (with $\Delta\beta = 0.31 \pm 0.05$) with the break in the NIR data could explain the SED at 0.7 d. By leaving slope difference $\Delta\beta$ as a free parameter, we still find that the SED is consistent with a single power law and there is no evidence of a shallower optical slope. The lower S/N of the NIR spectrum and further coverage hinder us to see such an optical break. Note that the *J-* and *H* -data are consistent with a single power law.

4.16 GRB 130606A

The X-shooter spectra of GRB 130606A ($z = 5.913$) afterglow were taken at 0.33 d after the burst. At ∼0.329 d after the burst trigger, the GROND photometric data in the $z'JH$ and K-band from GROND are taken from Afonso et al. (2013). The X-shooter data is scaled to the photometry. The NIR to the X-ray SED fits well with a single power law and no dust extinction with $A_V < 0.07$. Previously Hartoog et al. (2015), Japelj et al. (2015), and Bolmer et al. (2018) also found no dust extinction for this burst with $A_V < 0.2$.

4.17 GRB 131117A

The X-shooter spectra of GRB 131117A ($z = 4.042$) afterglow were taken at ∼0.05 d after the burst trigger. At ∼0.02 d after the burst, the GROND photometric data in the $i'z'J$ and H band from GROND were taken from Bolmer et al. (2018). The X-shooter data is scaled to the photometry at ∼0.02 d. The NIR to the X-ray SED provides a good fit with a broken power law and no dust extinction with $A_V <$ 0.11. Bolmer et al. (2018) reported no dust extinction for this burst with $A_V < 0.09$, consistent with our findings.

4.18 X-ray analysis

In Table 2, the equivalent hydrogen column densities ($N_{\rm H,X}$) derived through the simultaneous X-shooter to X-ray SED analysis for each GRB case is provided. For our time sliced spectra, we obtained significant $N_{\rm H,X}$ measurements for 10 cases only. We compared the $N_{\rm H,X}$ values with the redshift of GRBs. For our smaller sample, we find an evolution of the $N_{\rm H,X}$ with redshift as suggested by Campana et al. (2012). For measurements only, the statistical analysis results in a Spearman rank correlation coefficient $r = 0.89$ and >99 percent probability. The slope of the correlation is 0.40 ± 0.04. This is in contrast with the findings of Buchner, Schulze & Bauer (2017) suggesting no evolution of the $N_{\rm H,\,X}$ with redshift. Comparing $N_{\rm H,\,X}$ values of our sample with Buchner et al. (2017) indicates their values are up to 1.0 dex smaller.

5 DISCUSSION

5.1 Average grb extinction curve

Seven GRBs in our sample are consistent with no dust extinction and their 3σ A_V upper limits are provided in Table 2. 10 extinguished out of 17 GRBs have small to high extinction values with A_V values ranging from 0.11 ± 0.04 to 1.02 ± 0.11 resulting in a mean of $A_V = 0.27$ mag (standard deviation of 0.27). Covino et al. (2013) found from a sample of 58 GRBs that 50 per cent prefer less than 0.3–0.4 mag extinction. In our smaller sample, 94 per cent bursts have $\lesssim$ 0.3 mag extinction. Individual best-fitting extinction curves are shown as black full lines in Fig. 3, but as explained below we do not here include the three lowest redshift objects due to the shortened coverage in rest-frame UV. For comparison we also plot several standard extinction curves: the SMC extinction curve from Pei (1992), the flattest known SMC extinction curve (with c_1 = −4.94 ± 0.63, c_2 = 2.27 ± 0.20, c_4 = 0.18 ± 0.08, and R_V = 3.30 ± 0.38) towards sightline AzV 18 (Gordon et al. 2003), the SMC Bar extinction curve (c_1 = −4.96 ± 0.20, c_2 = 2.26 ± 0.04, c_4 = 0.46 ± 0.08, and R_V = 2.74 ± 0.13) from Gordon et al. (2003), and the steepest intrinsic QSO extinction curve (Zafar et al. 2015) derived for a sub-sample of High-A_V quasar (HAQ; Krogager et al. 2015) survey. Out of 10 dusty cases in our sample, three GRBs (GRB 100418A, GRB 111209A, and GRB 130427A) were at low redshifts ($z < 0.7$) and are therefore lacking rest-frame UV information of their extinction curves. Of the remaining seven cases, three GRB afterglows prefer extinction curves steeper than the typical Pei (1992) SMC curve (the three upper black curves in Fig. 3). However, R_V values rather than clustering around a particular value show a remarkably even distribution of R_V values bracketed by the AzV 18 and the HAQ curves. In particular, the histogram of R_V values of seven GRBs with broad coverage has a flat distribution between values ranging from 2.38 to 3.01 (see Table 2).

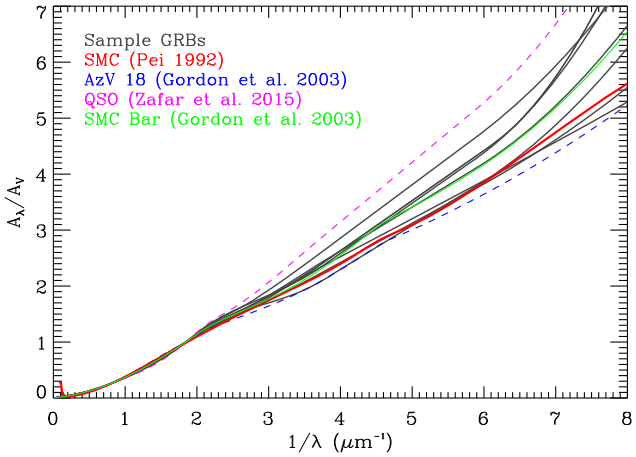

Figure 3. Individual extinction curves of 7 GRB afterglows with broadest wavelength coverage in our sample are compared with the extinction curve of the average SMC (red) taken from Pei (1992). For a comparison, the blue, green, and magenta dashed curves show the flattest SMC extinction curve towards sightline AzV 18, SMC Bar extinction curve (Gordon et al. 2003), and steepest QSO extinction curve (Zafar et al. 2015), respectively. GRB extinction curves derived in this work usually appear to be steeper than the typical SMC curve, however, have a broad range of R_V values.

To derive the *'average GRB extinction curve'* for our sample, we adopt two methods.The first method is to generate the *'average GRB extinction curve'* by calculating the *weighted mean* (*WM*) values of the best-fitting parameters. It is seen from the R_V measurements in Table 2 that the scatter of the distribution is much larger than the individual measurement errors, i.e. the scatter represents a real intrinsic distribution. For this reason we provide, in the bottom two rows of Table 2, both the *WM* and its corresponding error as well as the measured scatter (*Stddev*) of the distribution. As before, we again discard the three low-redshift GRBs (GRB 100418A, GRB 111209A, and GRB 130427A) and re-compute the *WM* values and corresponding errors. This results in $c_1 = -4.76 \pm 0.09$, $c_2 = 2.21 \pm 0.05$, $c_4 = 0.58 \pm 0.02$, and $R_V = 2.61 \pm 0.08$, identical to the values listed in Table 2) to within less than 1σ errors for all parameters, i.e. the final curve is not strongly influenced by those three objects. We then use these *WM* values to draw the red colour extinction curve in Fig. 4, where the red shaded area marks the combined uncertainty via propagation of errors on all parameters.

In our second method, we compute the *'average GRB extinction curve'*. i.e. the average of the actual individual curves rather than the parameters, but here only taking into account the 1/λ (μm^{-1}) wavelength range covered by each X-shooter observation. For each rest wavelength 1/λ (μm^{-1}) a mean and 1σ error on A_λ/A_V is computed. Because of the vastly different redshifts, the resultant mean extinction curve must display a series of 'steps' where each spectrum begins and ends. That curve is shown in Fig. 4 in black colour. The grey shaded area illustrates the 1σ error on the extinction curve.

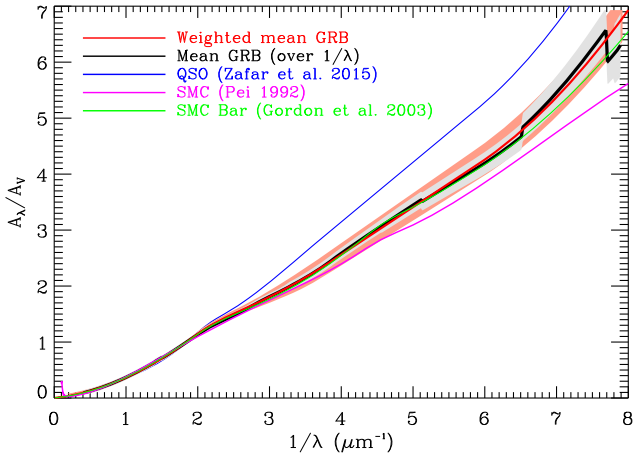

Figure 4. 'Average GRB extinction curves' computed using the *WM* values of seven extinguished GRBs (red) and by estimating the mean for each 1/λ (μm^{-1}) over the X-shooter observational coverage (black). The red and grey shaded areas represent the combined 1σ error on the averages (see Section 5.1 for more details on the computation methods). The magenta and green solid lines indicate the typical SMC (Pei 1992) and average SMC Bar (Gordon et al. 2003) extinction curves, respectively. The average steep QSO extinction curve from Zafar et al. (2015) is shown in blue solid line for a comparison.

As can be seen from the figure, the agreement between the results of the two methods is excellent. Hereafter, we shall refer to the *WM* extinction curve as the *'average GRB extinction curve'*. From Fig. 4 it is also seen that the *average GRB extinction curve* is slightly steeper than the canonical Pei (1992) SMC curve (with $R_V = 2.93$) but matches well with the SMC Bar extinction curve presented in Gordon et al. (2003).

Note that our sample contains five GRBs above $z > 4$. Only two of them have significant but small amount of dust (GRB 100219A: $A_V = 0.14 \pm 0.03$ and GRB 111008A: $A_V = 0.12 \pm 0.04$) while three (GRB 120923A: $A_V < 0.16$, GRB 130606A: $A_V < 0.07$, and GRB 131117A: $A_V < 0.11$) are consistent with no dust. These high-redshift cases are consistent with the findings of a decrease in dust content at $z > 4$ suggested by Zafar et al. (2011b) and recently confirmed by Bolmer et al. (2018).

5.2 Extinction curves comparison

None of our extinguished GRBs have a significant 2175 Å dust feature (but see Section 4.11). In Fig. 4 we plot a few featureless comparison extinction curves from the SMC and from QSOs. We use Kolmogorov–Smirnov statistics to determine the significance of the difference between the various extinction curves and find that the average intrinsic QSO extinction curve, derived for a HAQ survey sub-sample, from Zafar et al. (2015) with $R_V = 2.2 \pm 0.2$ deviates from the average GRB extinction curve at >99 per cent confidence level. The average GRB curve is similar to but slightly steeper than the typical Pei (1992) SMC extinction curve. It is consistent with the SMC bar extinction curve from Gordon et al. (2003) at the ∼95 per cent confidence level. We find that the SMC bar extinction curve (the green curve in Fig. 3 and 4) is on average a better representation of our sample.

Wiersema (2011) fitted hydrogen and helium fluxes of several recombination transitions seen in the spectra of GRB host galaxies to estimate R_V using the Cardelli et al. (1989) parametrization. The extinction over all recombination line regions combined, rather than one sightline (as in this work) resulted in R_V higher than the average MW value. Previously, Schady et al. (2012) attempted to fit the parametric extinction curve to the GRB X-ray to optical/NIR photometric data. For moderately extinguished GRBs ($A_V < 1$), their best-fitting Fitzpatrick & Massa (1990) extinction curve is closer to the LMC ($R_V = 3.16$). Although due to the absence of a 2175 Å bump, the extinction model around the bump location is closer to the featureless SMC curve. 12 per cent of the 49 GRBs in their sample are significantly dusty with $A_V > 1$ and found to have extinction curves flatter than the mean MW extinction curve. In our sample, we only have GRB 120119A with $A_V \gtrsim 1$, where the bump location falls between the edges of the UVB and VIS arms. Therefore, we are not able to determine whether or not a bump is present. For the moderate extinction cases, we also find that the GRB SEDs are better described by featureless extinction curves.

A 2175 Å bump extinction curve with steep UV slope was found for GRB 080605 (Zafar et al. 2012). For GRB 140506A, Fynbo et al. (2014) reported an extremely steep UV extinction curve that could be fitted by a Fitzpatrick & Massa (2007) parametrization of an extreme 2175 Å bump, albeit with fitting parameters unlike any derived for MW sight-lines. Heintz et al. (2017) later excluded this possibility and the extinction curve of GRB 140506A must hence be very steep for other reasons. Zhou et al. (2006) reported a steeper extinction law for a sample of ∼2000 UV-deficient narrow line Seyfert galaxies. Leighly et al. (2014) found a steep extinction law with $R_V = 2.74$ for the Seyfert galaxy Mrk 231 using the equation from Goobar (2008). Gallerani et al. (2010) found for $3.9 < z < 6.4$ QSOs that their extinction curves deviate from the SMC law and flatten at $\lambda_{rest} < 2000$ Å. In contrast, for a sample of QSOs at $z \sim 6$, Hjorth et al. (2013) suggested that the median extinction curve is consistent with the featureless SMC curve. Recently for the HAQ survey sub-sample at $0.7 < z < 2.1$, Zafar et al. (2015) fitted a parametric extinction law and found that an SMC law is inadequate to define SEDs of those dusty QSOs. Their entire sample is well fit with a single best-fitting value of $R_V = 2.2 \pm 0.2$. An even steeper extinction curve with $R_V = 1.4$ is proposed for the Type Ia supernova SN 2014JA in the starburst galaxy M82 (Amanullah et al. 2014), remarkably similar to that derived for GRB 140506A (Heintz et al. 2017). Zelaya et al. (2017) found that weighted average R_V of ten Type Ia SNe is $R_V = 1.5 \pm 0.06$. They further find higher continuum foreground polarization (by dust scattering) and hence A_V for low R_V values. Circular polarization intrinsic to the source or by dust scattering effects along the line of sight is found for GRB 121024 (Wiersema et al. 2014). We here have a direct measure of the R_V values in young star-forming galaxies, finding slightly steeper extinction curves but no evidence for very low R_V.

Exploiting the broad wavelength coverage of X-shooter we are here able to fit the individual extinction curves of GRBs for the first time. The GRB afterglows have a continuum of extinction curves and are on average slightly steeper than the canonical SMC.

5.3 Dust composition

Our GRB extinction curves do not have a significant 2175 Å dust feature implying an absence of carbonaceous grains. Using the X-shooter data, we have enough coverage available to detect a significant 2175 Å bump but we did not discover any. It is possible that these GRB environments have small carbonaceous grains but that the steepness of the curve dilutes the feature. The steep extinction curve indicates the presence of small grains which could be due to the destruction of dust by the harsh environment (Reach et al. 2000) of the GRB or due to GRB stellar environments being

young age and/or of lower metallicities. For the first scenario, dust destruction in the ISM could be caused by sputtering, evaporative heating, and/or grain charging, where destruction rate depends on grain size and composition. Fruchter, Krolik & Rhoads (2001) modelled the influence of different effects on dust in GRB environments and find that grain shattering could reduce the total extinction for $\lambda < 1400$ Å. Perna, Lazzati, and Fiore (2003) simulated dust destruction due to thermal sublimation of the dust grains resulting in a significant reduction of the 2175 Å bump and as the destruction proceeds, the extinction curve rather becomes flatter. For the second scenario of small grain presence, we looked in our sample where R_V values and metallicities are reported. We find that metallicities are available only for five dusty GRBs in our sample: GRB 100219A ($[M/H) = -1.1 \pm 0.2$; Thöne et al. 2013), GRB 111008A ($[M/H] = -1.7 \pm 0.1$; Sparre et al. 2014), GRB 120119A ($[M/H] = -0.79 \pm 0.25$; Wiseman et al. 2017), GRB 120815A ($[M/H] = -1.15 \pm 0.12$; Krühler et al. 2013), and GRB 121024A ($[M/H = -0.7 \pm 0.1$; Friis et al. 2015). Although low number statistics, comparing metallicities with R_V indicates that data are linearly correlated with a coefficient $r = 0.73$. A larger sample of metallicities and total-to-selective extinction values will better infer the relation between both quantities.

Mathis (1996) proposed that steeper extinction curves could arise due to the presence of silicate grains. ∼70 per cent of the interstellar dust core mass is composed of silicate grains (Draine 2003). For the cases where both a 2175 Å bump and UV steep rise is present, Li and Draine (2001) andWeingartner & Draine (2017) modelled that far-UV extinction could be due to a population of both small carbon and silicates grain. The steep extinction curves observed in this work could be due to such small grains.

6 CONCLUSIONS

We present here a sample of X-shooter selected GRB afterglow SEDs from March 2009 to March 2014. We analyse the NIR to X-ray SEDs of 17 GRB afterglows with redshifts ranging from $0.34 < z < 7.84$. We have only included GRBs for which nearly simultaneous photometry is available allowing us to proper flux calibrate the X-shooter data. Single and broken (with a change in slope fixed to $\Delta\beta = 0.5$) power laws are used to fit the SEDs together with the analytical FM extinction law. 10 out of the 17 GRBs are found to be extinguished with A_V values ranging from $A_V = 0.1 - 1.0$ mag with a mean of $A_V = 0.27$ mag. Our individual R_V values have a flat distribution with values varying from 2.38–3.01. The flat distribution on R_V's indicates that GRBs have a wide range of grain sizes and compositions, but on average favouring a somewhat steeper reddening than the standard SMC. We derived the 'average GRB extinction curve' by obtaining the weighted mean values of the best-fit parameters of seven individual curves (chosen to have the broadest wavelength coverage) resulting in an optimal weighted combined value of $R_V = 2.61 \pm 0.08$. This extinction curve is similar to, but slightly steeper than, the typical Pei (1992) SMC curve. It is fully consistent with the SMC Bar from Gordon et al. (2003) at ∼95 per cent confidence level. Steeper extinction curves have been previously reported for GRBs, Seyfert galaxies, Supernovae, and QSOs. Steep extinction curves are thought to be representative of a population of silicates producing small size dust grains. Large dust grains may be destroyed in harsh environments of GRBs, resulting in steep extinction curves. Another possibility could be young age and/or lower metallicities of GRBs, although statistics are low.

ACKNOWLEDGEMENTS

The X-ray data for this work is obtained from the UK *Swift* Science Data Center at the University of Leicester. KEH acknowledges support by a Project Grant (162948-051) from The Icelandic Research Fund. AdUP acknowledges support from the Spanish research project AYA 2014-58381-P, from a RyC fellowship and from a BBVA Foundation grant for Researchers and Cultural Creators. JJ acknowledges support from NOVA and NWO-FAPESP grant for advanced instrumentation in astronomy.

REFERENCES

Afonso P., Kann D. A., Nicuesa Guelbenzu A., Kruehler T., Elliott J., Greiner J., 2013, GRB Coordinates Network, 14807
Amanullah R. et al., 2014, ApJ, 788, L21
Anders E., Grevesse N., 1989, Geochim. Cosmochim. Acta, 53, 197
Arnaud K. A., 1996, in Jacoby G. H., Barnes J., eds, ASP Conf. Ser., Vol. 101, Astronomical Data Analysis Software and Systems V, Astron. Soc. Pac., San Francisco, p. 17
Beuermann K. et al., 1999, A&A, 352, L26
Bohren C. F., Huffman D. R., 1983, Absorption and scattering of light by small particles. Wiley, New York, p. 227
Bolmer J., Greiner J., Krühler T., Schady P., Ledoux C., Tanvir N. R., Levan A. J., 2018, A&A, 609, A62
Buchner J., Schulze S., Bauer F. E., 2017, MNRAS, 464, 4545
Burrows D. N. et al., 2005, Space Sci. Rev., 120, 165
Campana S. et al., 2012, MNRAS, 421, 1697
Cardelli J. A., Clayton G. C., Mathis J. S., 1989, ApJ, 345, 245
Covino S. et al., 2013, MNRAS, 432, 1231
D'Elia V. et al., 2010, A&A, 523, A36
de Ugarte Postigo A., Thöne C. C., Goldoni P., Fynbo J. P. U. X-shooter GRB Collaboration., 2011, Astron. Nachr., 332, 297
de Ugarte Postigo A., et al., 2018, A&A, submitted
Draine B. T., 2003, ARAA, 41, 241
Elíasdóttir, Á. et al., 2009, ApJ, 697, 1725
Evans P. A. et al., 2009, MNRAS, 397, 1177
Fitzpatrick E. L., Massa D., 1990, ApJS, 72, 163
Fitzpatrick E. L., Massa D., 2007, ApJ, 663, 320
Friis M. et al., 2015, MNRAS, 451, 167
Fruchter A., Krolik J. H., Rhoads J. E., 2001, ApJ, 563, 597
Fynbo J. P. U. et al., 2014, A&A, 572, A12
Galama T. J. et al., 1998, Nature, 395, 670
Gallerani S. et al., 2010, A&A, 523, A85
Gehrels N. et al., 2004, ApJ, 611, 1005
Gehrels N., Ramirez-Ruiz E., Fox D. B., 2009, ARA&A, 47, 567
Goobar A., 2008, ApJ, 686, L103
Gordon K. D., Clayton G. C., Misselt K. A., Landolt A. U., Wolff M. J., 2003, ApJ, 594, 279
Greiner J. et al., 2011, A&A, 526, A30
Haislip J. et al., 2010, GRB Coordinates Network, 10494
Hartoog O. E. et al., 2013, MNRAS, 430, 2739
Hartoog O. E. et al., 2015, A&A, 580, A139
Heintz K. E. et al., 2017, A&A, 601, A83
Hjorth J. et al., 2003, Nature, 423, 847
Hjorth J., Vreeswijk P. M., Gall C., Watson D., 2013, ApJ, 768, 173
Japelj J. et al., 2015, A&A, 579, A74
Kalberla P. M. W., Burton W. B., Hartmann D., Arnal E. M., Bajaja E., Morras R., Pöppel W. G. L., 2005, A&A, 440, 775
Kann D. A. et al., 2010, ApJ, 720, 1513
Krogager J.-K. et al., 2015, ApJS, 217, 5
Krühler T. et al., 2013, A&A, 557, A18
Leighly K. M., Terndrup D. M., Baron E., Lucy A. B., Dietrich M., Gallagher S. C., 2014, ApJ, 788, 123
Levan A. J. et al., 2014, ApJ, 781, 13
Li A., Draine B. T., 2001, ApJ, 554, 778

Li A., Liang S. L., Kann D. A., Wei D. M., Klose S., Wang Y. J., 2008, ApJ, 685, 1046
Liang S. L., Li A., 2009, ApJ, 690, L56
Marshall F. E. et al., 2011, ApJ, 727, 132
Mathis J. S., 1996, ApJ, 472, 643
Melandri A. et al., 2010, ApJ, 723, 1331
Mishra A., Li A., 2017, ApJ, 850, 138
Modigliani A. et al., 2010, Silva D. R., Peck A. B., Soifer T., Proc. SPIE Conf. Ser. Vol. 7737, Observatory Operations: Strategies, Processes, and Systems III. SPIE, Bellingham, p. 773728
Morgan A. N. et al., 2014, MNRAS, 440, 1810
Nardini M. et al., 2014, A&A, 562, A29
Pei Y. C., 1992, ApJ, 395, 130
Perley D. A. et al., 2011, AJ, 141, 36
Perley D. A. et al., 2014, ApJ, 781, 37
Perna R., Lazzati D., Fiore F., 2003, ApJ, 585, 775
Rau A. et al., 2010, ApJ, 720, 862
Reach W. T., Boulanger F., Contursi A., Lequeux J., 2000, A&A, 361, 895
Sari R., Piran T., Narayan R., 1998, ApJ, 497, L17
Schady P. et al., 2012, A&A, 537, A15
Schlafly E. F., Finkbeiner D. P., 2011, ApJ, 737, 103
Schlegel D. J., Finkbeiner D. P., Davis M., 1998, ApJ, 500, 525
Selsing J., et al., 2018 , A&A, preprint (arXiv:.1802.07727)
Sparre M. et al., 2011, ApJ, 735, L24
Sparre M. et al., 2014, ApJ, 785, 150
Starling R. L. C. et al., 2011, MNRAS, 411, 2792
Stratta G., Maiolino R., Fiore F., D'Elia V., 2007, ApJ, 661, L9
Stratta G., Gallerani S., Maiolino R., 2011, A&A, 532, A45
Stratta G. et al., 2013, ApJ, 779, 66
Tanvir N. R. et al., 2017, preprint (arXiv:1703.09052)
Thöne C. C. et al., 2013, MNRAS, 428, 3590
Varela K. et al., 2016, A&A, 589, A37
Vernet J. et al., 2011, A&A, 536, A105
Watson D., 2011, A&A, 533, A16
Watson D. et al., 2013, ApJ, 768, 23
Weingartner J. C., Draine B. T., 2001, ApJ, 548, 296
Wiersema K., 2011, MNRAS, 414, 2793
Wiersema K. et al., 2014, Nature, 509, 201
Willingale R., Starling R. L. C., Beardmore A. P., Tanvir N. R., O'Brien P. T., 2013, MNRAS, 431, 394
Wilms J., Allen A., McCray R., 2000, ApJ, 542, 914
Wiseman P., Schady P., Bolmer J., Krühler T., Yates R. M., Greiner J., Fynbo J. P. U., 2017, A&A, 599, A24
Xu D. et al., 2013, ApJ, 776, 98
Zafar T., Watson D. J., Malesani D., Vreeswijk P. M., Fynbo J. P. U. , Hjorth J., Levan A. J., Michalowski M. J., 2010, A&A, 515, A94
Zafar T., Watson D., Fynbo J. P. U., Malesani D., Jakobsson P., de Ugarte Postigo A., 2011a, A&A, 532, A143
Zafar T., Watson D. J., Tanvir N. R., Fynbo J. P. U., Starling R. L. C., Levan A. J., 2011b, ApJ, 735, 2
Zafar T. et al., 2012, ApJ, 753, 82
Zafar T. et al., 2015, A&A, 584, A100
Zelaya P. et al., 2017, ApJ, 836, 88
Zhou H., Wang T., Yuan W., Lu H., Dong X., Wang J., Lu Y., 2006, ApJS, 166, 128

This paper has been typeset from a TEX/LATEX file prepared by the author.